J. Comp. App. Res. Mech. Eng. Vol. 15. No. 1, pp. 51-61, 2025 *DOI: 10.22061/jcarme.2025.12184.2660*

SRTTU

Journal of Computational and Applied Research in Mechanical Engineering

jcarme.sru.ac.ir

JCARME

ISSN: 2228-7922

Research paper

Microstructural analysis of nickel-based CMSX-4 superalloy after electrochemical machining

A. Mehrvar[a,*], AR. Mirak[b] and M. Motamedi[a]

[a]*Department of Mechanical Engineering, Shahreza Campus, University of Isfahan, Iran.*
[b]*Faculty of Materials Engineering, Iran University of Science and Technology, Tehran, Iran.*

Article info:

Article history:

Received: 27/06/2025

Revised: 03/11/2025

Accepted: 10/11/2025

Online: 15/11/2025

Keywords:

Electrochemical machining,

CMSX-4 superalloy,

Microstructure,

SEM,

EDS.

[*]Corresponding author:
a.mehrvar@shr.ui.ac.ir

Abstract

Electrochemical machining (ECM) is an effective method for machining CMSX-4 superalloy, a single-crystal nickel-based superalloy, due to its unique performance in metal machining. The microstructure of this superalloy consists of three phases: gamma (γ), gamma prime (γ'), and carbide. The gamma prime phase is distributed cubically and homogeneously in the gamma field without any boundaries. It is essential to maintain this microstructure after the production process is completed. In the present study, ECM was performed on a CMSX-4 superalloy workpiece. The microstructure of the workpiece was then investigated before and after ECM using scanning electron microscopy and energy-dispersive spectroscopy analysis from two sides. The results showed that no changes were observed in the CMSX-4 microstructure after the ECM process. The single-crystal structure and the distribution of the gamma prime phase were maintained after this machining process, indicating that ECM is an effective machining method for CMSX-4 superalloy without compromising its critical microstructural features.

1. Introduction

Electrochemical machining (ECM) is a highly efficient and cost-effective method in the realm of non-traditional machining. This process relies on the principles of electrolysis and electrochemical dissolution to remove material from the workpiece [1-4].

In ECM, the workpiece is connected to the positive pole (anode), while the tool serves as the negative pole (cathode) of a direct current power supply. As the tool moves towards the workpiece, a narrow gap, known as the machining gap, is created between the anode and cathode. An electrically conductive electrolyte is then pumped into this gap, completing the electrical circuit and facilitating the flow of electrons [1-4].

As the electrons move through the circuit and ions are separated from the surface of the workpiece, a process known as anodic dissolution occurs. This dissolution follows the

Faraday relationship and results in the formation of hydrogen gas around the tool [1-4].

One of the key advantages of ECM is the absence of direct contact between the tool and the workpiece. This eliminates the risk of surface stresses and avoids the problems associated with the heat-affected zone, which can be a drawback in other machining methods such as electrical discharge machining (EDM) [5-7]. Moreover, the hardness and toughness of the workpiece material have no impact on the ECM process, and the tool does not experience any wear during this process [5-7].

CMSX-4 is a second-generation, rhenium-bearing nickel-based single crystal superalloy that offers superior properties for advanced gas turbine engine components. Compared to earlier superalloys, CMSX-4 has improved creep-rupture, fatigue, oxidation, and coating performance, resulting in enhanced turbine engine durability and efficiency [8-13].

The single crystal structure of CMSX-4 eliminates grain boundaries, which are typically a weakness in polycrystalline superalloys at high operating temperatures. CMSX-4 also contains reactive element additions such as lanthanum and yttrium, which further enhance its high-temperature properties [8-13]. However, limited research has been conducted on the ECM of this specialized nickel-based superalloy [14-16]. The following is some research on the ECM machining of superalloys, especially nickel-based ones.

Klocke *et al.* [17] investigated the electrochemical machining (ECM) of nickel and titanium-based superalloys commonly used in jet engine components such as blades and discs. The study focused on optimizing tool design and determining the electrochemical dissolution rate based on the tool feed rate and current density. The researchers examined several nickel-based superalloys, including Inconel 718, Inconel 718 DA, Waspaloy, René 88, and IN 100, but did not include any single-crystal superalloys. As a result, a good ECM behavior and effective machining rate were reported.

In another study, electrochemical machining has proven to be an efficient technique for selective machining to separate stainless steel from Ti-6Al-4V alloy. Two different electrolyte solutions were studied. The first electrolyte selectively removed only the stainless-steel component. The second electrolyte not only removed the stainless steel but also eliminated the layer formed by steel-titanium intermetallic phases [18].

Niu *et al.* [19] conducted a study on the electrochemical machining of the GH4169/ Inconel 718 superalloy. Their findings suggest that increasing the feed rate during ECM can enhance the machining rate, surface quality, and uniformity of the machining gap.

Additionally, they proposed a jet electrolyte flow method for electrochemical milling on this nickel-based superalloy, which demonstrates high productivity and stability, particularly suitable for deep-depth machining applications [19].

In another study, the enhancement of platform precision and the minimization of stray current in the ECM process with auxiliary tools in the cathode for blade profiles were examined using three materials: SS304, Inconel 718, and TiAl 4822 [20].

The cathode (tool) was designed in three configurations: without insulation or auxiliary tools, with cathode insulation, and with a combination of cathode insulation and ECM auxiliary tools. The findings showed that the use of auxiliary tools significantly improves platform accuracy and reduces unnecessary machining [20].

Furthermore, the effect of electrolyte flow on the ECM machining of blisk was investigated both numerically and experimentally. Modifying the electrolyte flow mode enhanced the performance of the ECM process for blisk machining by up to 70% [21].

In addition, Mouliprasanth and his colleague's primary objective in this research is to assess the impact of scale on the ECM process of Nitinol alloy. The study aims to transfer machining parameters from the micro to the macro scale. Tool feedrate, duty ratio, and voltage are considered as process input parameters, while machining rate and geometric features serve as the response variables [22].

Ge *et al.* [23] conducted a study on the electrochemical dissolution behavior of the K423A nickel-based superalloy in a sodium

nitrate electrolyte. Their findings highlight that ECM is a promising technique for machining nickel-based superalloys. The study revealed that sodium nitrate outperforms sodium chloride as an electrolyte, with an optimal concentration of 10% for enhanced performance. Ultimately, the ECM method is presented as an effective and cost-efficient process for machining the K423A nickel-based superalloy [23]. Additionally, Wang *et al.* [24] proposed a method to enhance local machining in the electrochemical machining process. This approach involves synchronizing the pulse power supply with low-frequency oscillations of the tool. As a result, the on and off positions of the pulse power supply are aligned symmetrically with the tool's feedrate wave. Simulations and experiments conducted on rhombus-shaped holes demonstrated improvements in both surface accuracy and quality [24].

Bilgi *et al.* [25] conducted a study on drilling nickel-base superalloys using the electrochemical machining method. They proposed effective solutions to address challenges associated with ECM processes for large blades with torsion angles and two-sided platforms.

Additionally, the optimal feedrate of the cathodes towards the blade was established. Additionally, a new method has been proposed for flushing the electrolyte in the machining gap on both sides of the blades and cathodes, demonstrating excellent results in both simulations and experiments [26].

Huang and Liu [27] investigated micro-electrochemical machining (micro-ECM) to fabricate intricate shapes on nickel-based superalloys. They achieved the creation of complex micro-dimensional geometries through the application of nanoscale voltage pulses. The study focused on various parameters, including voltage, pulse on-time, and electrode diameter, ultimately leading to the successful machining of complex shapes [27].

Burger *et al.* [28] conducted a study on the ECM of the LEK94 single-crystal superalloy. Their research identified current density as the most critical and effective parameter for enhancing surface quality during the machining process. Current density is influenced by several factors, including the machining gap, voltage, and electrolyte conductivity.

The findings indicated that low current density results in non-uniform dissolution of the superalloy, leading to increased surface roughness. Conversely, achieving a high current density is essential for promoting uniform electrochemical dissolution, which in turn facilitates a higher machining rate and reduces surface roughness in this nickel-based superalloy [28]. Moreover, Singh *et al.* [29] analyzed the microstructure and multi-objective optimization of the ECM of Inconel 825 superalloy using a hybrid method.

The voltage, electrolyte concentration, and tool feedrate were considered as optimization inputs, while machining removal rate, surface roughness, and extra machining were the objective functions. The optimal machining conditions were determined to be a voltage of 16 volts, an electrolyte concentration of 45 g/l, and a tool feedrate of 0.3 mm/min [29].

The surface integrity of three types of γ-TiAl alloy was examined after ECM by Wang et al. [30]. The study utilized two levels of current density to compare the effects of low and high process current densities on the surface properties of the alloy. It was found that machining at low current densities led to local corrosion and rough surfaces, whereas high current densities produced smooth surfaces across all three alloys [30].

This research examines the microstructure of the CMSX-4 nickel-based single-crystal superalloy, focusing on its characteristics before and after electrochemical machining (ECM). Scanning electron microscopy (SEM) images, captured from both the front and side views of the workpiece surface, reveal that the single-crystal microstructure remains unchanged following the ECM process. This finding is significant for understanding the effects of ECM on the structural integrity of this advanced superalloy.

2. Materials

2.1. Workpiece

The workpiece was made of a nickel-based single-crystal superalloy, which has unique properties. Its chemical composition is listed in

Table 1. This material exhibits high hardness and strength. However, machining it using traditional and modern methods poses challenges such as tool wear, residual thermal and mechanical stresses, heat-affected zones (HAZ), and maintaining surface accuracy and quality. A CMSX-4 nickel-based superalloy was produced using vacuum induction melting (VIM). A laboratory Bridgman furnace equipped with a water-cooling system was used for the directional freezing. Subsequently, the single-crystal samples underwent a precipitation hardening heat treatment involving dissolution annealing and aging processes. Fig. 1 shows a cast ingot of this material, which was ground and then cut into 2 mm-thick tablets.

2.2. Tool and electrolyte

The tool is made of brass with a diameter of 6 mm. Furthermore, the tip of the tool was polished and ground to eliminate any turning effects and to create a smooth surface. Three of these tools were made, with an alternative tool available in the case of damage during the experiments.

The side of the tool was insulated to prevent the adverse effects of stray currents. Fig. 2 shows that the negative and positive poles were connected to the tool and workpiece, respectively. This machine can flush the electrolyte either parallel (from the sidewalls of the working chamber) or perpendicular (inside the tool) to the workpiece surface. Electrolytes are one of the main components of the ECM process. The uniformity and purity of the electrolyte are important during machining.

The metals removed from the workpiece and impurities in the electrolyte can increase the risk of sparks, alter the machining rate, and require a proper purification and filtration system in the machine. The electrolyte used was a sodium nitrate solution with a concentration of 80 g/l.

3. Experimental details

The experiments were performed according to the range specified for the input parameters of the electrochemical machining process based on previous studies [11, 12].

Table 1. Chemical composition (wt%) of CMSX-4 workpiece.

Content	Element					
	Ni	Co	Cr	Ta	W	Al
Min	Rem.	9.3	6.4	6.3	6.2	5.45
Max		10	6.6	6.7	6.6	5.75
	Re	Ti	Mo	Hf	Nb	C
Min	2.8	0.9	0.5	0.07		
Max	3.1	1.1	0.7	0.12	0.1	0.08
	Si	Mn	V	P	Fe	Cu
Min						
Max	0.04	0.01	0.01	0.015	0.015	0.005

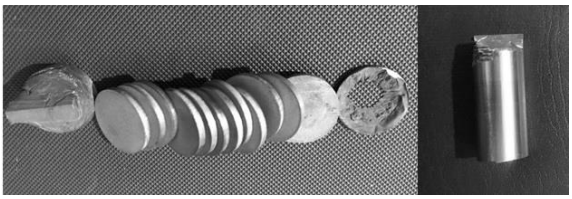

Fig. 1. CMSX-4 workpiece as heat treatment.

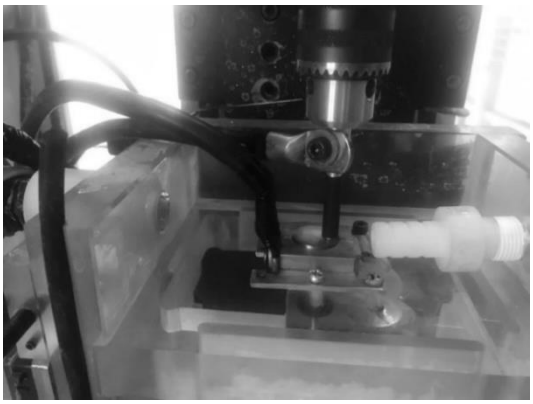

Fig. 2. Electrochemical machining chamber with tool and workpiece.

An ECM machine with high flexibility and reproducibility is needed to perform practical testing and develop electrochemical machining technology. A device with a 30-volt voltage and a 108-ampere current was used. This machine consists of four separate units: the machine, power supply, electrolyte, and control units that interact with each other through special integration. This machine is developed by considering the measurement units and suitable monitoring for performing experiments and acquiring technical knowledge for electrochemical machining. Fig. 3 shows an image of this machine.

Fig. 3. The electrochemical machining machine.

3.1. Sample and fixture preparations

Unfortunately, this material lacks magnetic properties, making it difficult to block and grind. The workpiece, with a thickness of 2 mm, was cut using wire electrical discharge machining (WEDM) and then ground. The use of Plexiglas as the chamber material is a good choice, as it provides the necessary insulation and chemical resistance, while also allowing for improved visibility during the process. The transparency of the Plexiglas chamber can be particularly beneficial for monitoring and troubleshooting sample preparation steps.

3.2. Implementation of experiments

Finally, machining was performed on the workpiece after adjusting the input parameters of the process, such as voltage, machining time, and initial gap. The experimental parameters were adjusted as indicated in Table 2.

3.3. SEM / EDS testing

After polishing, the samples were prepared using alumina powders with particle sizes ranging from 0.05 to 0.2 µm to observe the dendritic microstructure of the cross-sections. A marble etchant solution was used to reveal the microstructure of the sample.
The microscopic structure of the samples was evaluated using a Nikon EPIPHOT 300 optical microscope equipped with a SONY camera, as well as SEM PHILIPS XL30 and FE-SEM TESCAN MIRA3.

Table 2. The ECM process parameters.

Process parameter	Value
Voltage	25 V
Machining gap	150 µm
Tool feed rate	0.12 mm/min
Electrolyte concentration	80 gr/l
Electrolyte conductivity	88.8 mS/cm
Time of machining	30 s

4. Results and discussion

4.1. Workpiece movement measurement

Fig. 4 was created using a video measuring machine (VMM) to measure and plot the movement of the workpiece during the experiments. As shown in Fig. 4, the workpiece was cut from the middle using WEDM after 30 s of ECM.
In this study, the microstructure of the workpiece was investigated from two sides using SEM and energy-dispersive X-ray spectroscopy (EDS) in two different modes:

1. Without ECM (F1 and T1 in Fig. 4)
2. After ECM (F2 and T2 in Fig. 4)

The two sides were analyzed as follows:

1. Top view (T1 and T2 in Fig. 4)
2. Front view (F1 and F2 in Fig. 4)

This comprehensive microstructural analysis provided valuable insights into the effects of the ECM process on the workpiece material.

4.2. Investigation of the machining surface's microstructure before and after ECM

The microstructure was studied in two different sections before and after ECM operations. First, the surface was analyzed using SEM images before and after machining.

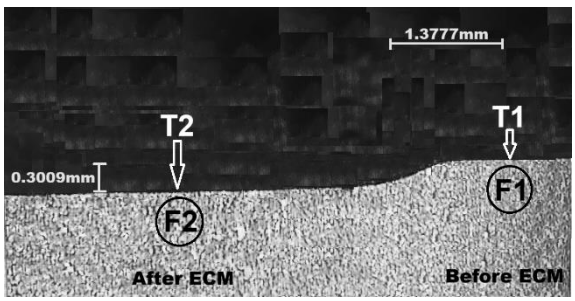

Fig. 4. Image of workpiece with video measuring machine (mm).

Fig. 5 indicates the pre-machined surface (T1 according to Fig. 4), while Fig. 6 shows the microstructure images after ECM (T2 according to Fig. 4). Fig. 5 shows the pre-machined surface (T1) of the nickel-based superalloy. The SEM analysis reveals a complex microstructure composed of three main phases:

1. Gamma (γ) field phase: The continuous matrix phase [11].
2. Gamma prime (γ') strengthening phase: Coherent precipitates that enhance the strength of the alloy [11].
3. Carbide Phase: A small amount of dispersed carbide particles, typically rich in refractory elements such as tungsten, tantalum, or titanium, which help strengthen the alloy [11].

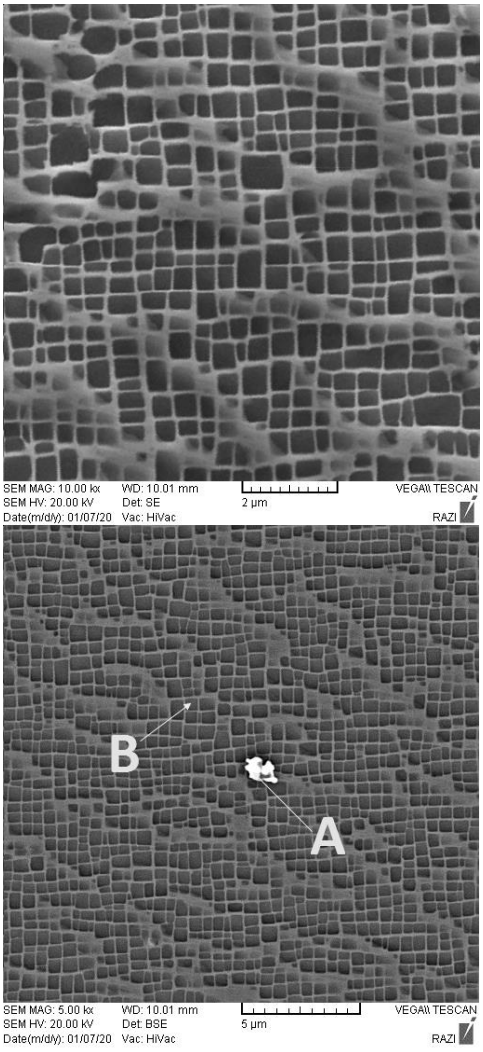

Fig. 5. Microstructure of the surface before the ECM process (view T1 according to Fig. 4).

Fig. 6 shows the microstructure of the surface after ECM (T2 in Fig. 4). The SEM analysis reveals that the three main phases (γ, γ', and carbides) are still present, and their distribution and characteristics appear to be similar to the pre-machined surface (T1). The complex microstructure of the nickel-based superalloy, with its combination of the γ, γ', and carbide phases, contributes to the alloy's exceptional high-temperature strength and creep resistance, making it suitable for critical components in gas turbine engines [14]. Tables 3 and 4 present the EDS analysis of points A and B in Fig. 5 and Fig. 6, respectively. The EDS data reveal the composition and identity of the key phases present in the superalloy microstructure [12].

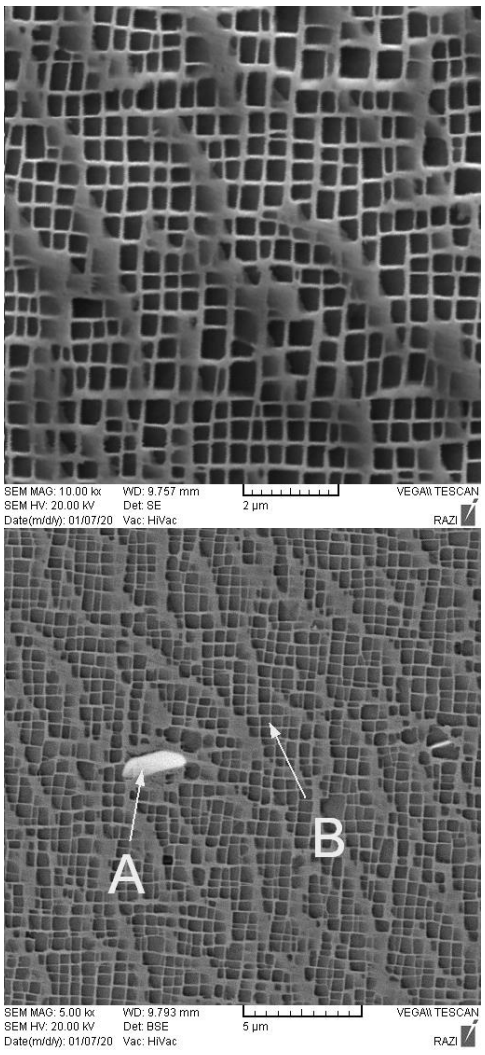

Fig. 6. Microstructure of the surface after the ECM process (view T2 according to Fig. 4).

Table 3. The EDS analysis of points A and B in Fig. 5.

Element	Series	Point A (wt.%)	Point B (wt.%)
Carbon	K series	8.16	-
Titanium	K series	17.52	1.16
Chromium	K series	5.21	5.43
Cobalt	K series	4.21	7.63
Nickel	K series	27.49	61.94
Tantalum	L series	37.42	8.25
Aluminum	K series	-	5.53
Iron	K series	-	0.31
Tungsten	L series	-	4.46

Table 4. The EDS analysis of points A and B in Fig. 6.

Element	Series	Point A (wt.%)	Point B (wt.%)
Carbon	K series	5.15	-
Titanium	K series	11.76	0.73
Chromium	K series	6.54	4.75
Cobalt	K series	5.37	8.22
Nickel	K series	36.78	58.48
Tantalum	L series	34.41	11.55
Aluminum	K series	-	3.02
Iron	K series	-	0.71
Molybdenum	L series	-	2.04
Tungsten	L series	-	10.48

According to the EDS analysis, the white dots labeled A in the SEM images correspond to carbide phases containing titanium and tantalum. Additionally, the gamma prime (γ') phase appears as homogeneously distributed, cuboidal precipitates within the gamma (γ) matrix at very short inter-particle distances [12]. Point B in the EDS analysis has a higher nickel content, indicating it is located within the γ matrix phase. The γ phase is the continuous matrix phase that surrounds the γ' precipitates [12]. Comparison of the SEM images before and after ECM shows that the superalloy microstructure remains unchanged by the machining process.

The three main phases - γ, γ', and carbides - are still present in the post-ECM microstructure. The relative amounts and distributions of these phases are crucial for the superalloy's high-temperature mechanical properties and oxidation resistance [12].

4.3. Investigation of the lateral surface microstructure before and after ECM

The SEM images of the lateral surface (F1 and F2 in Fig. 4) are presented to investigate the microstructural changes before and after ECM. Fig. 7 shows the SEM image of the microstructure before ECM, while Fig. 8 depicts the microstructure after the ECM process. As shown in Fig. 7, the microstructure before ECM consists of γ and γ' phases. Additionally, carbide phases are present in the form of large and heterogeneous particles dispersed throughout the microstructure [14]. The EDS analysis in Table 5 confirms the presence of the carbide phase at points A and B, as shown in the microstructure in Fig. 7. The SEM image in Fig. 8 reveals that the microstructure after ECM also includes γ and γ' phases [14]. The EDS analysis in Table 6 shows that point A in Fig. 8 corresponds to the carbide phase, which is consistent with the findings before ECM.

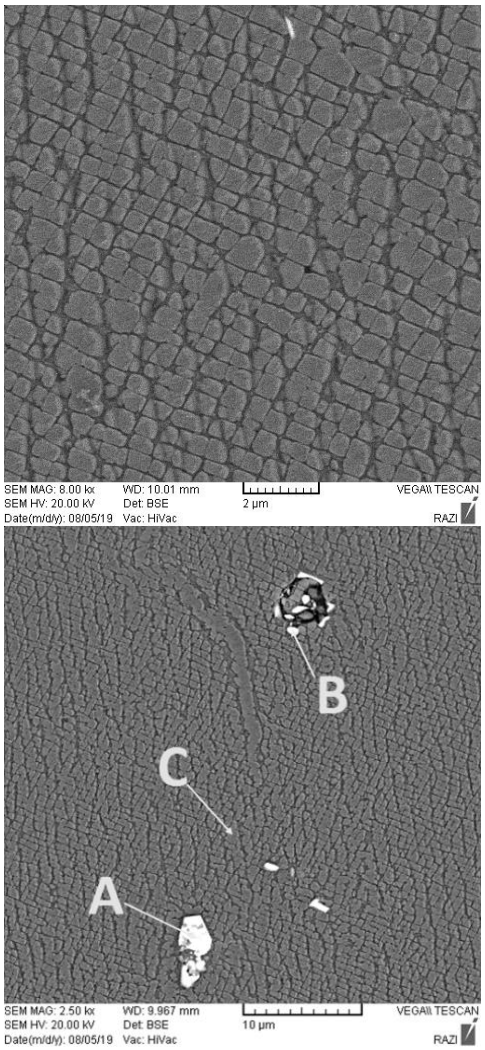

Fig. 7. Microstructure of the lateral surface before the ECM process (view F1 according to Fig. 4).

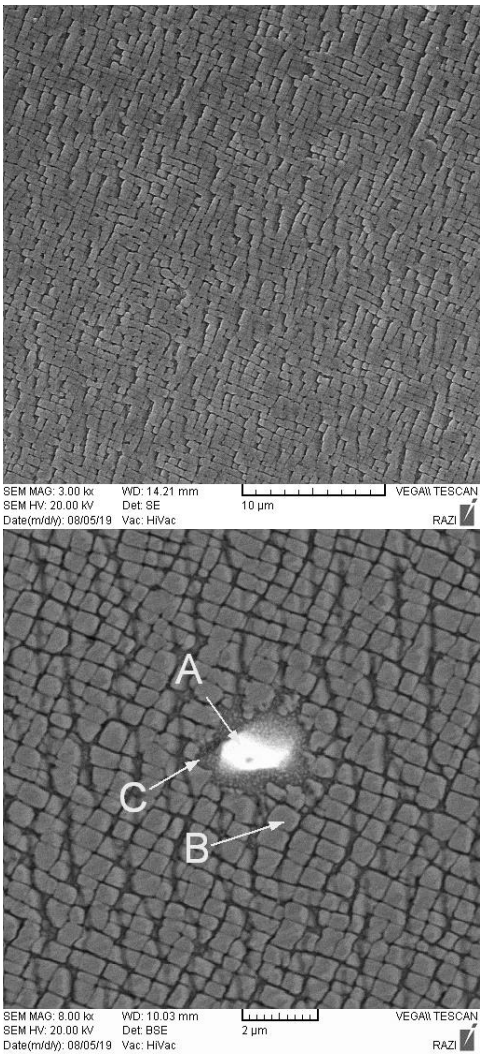

Fig. 8. Microstructure of the lateral surface after the ECM process (view F2 according to Fig. 4).

Point B in Table 6 represents the γ phase, while point C indicates the γ' phase [14]. The lower nickel content at point C compared to point B suggests that point C corresponds to the γ' phase in Fig. 8.

Table 5. The EDS of points A, B, and C in Fig. 7.

Element	Series	A (wt.%)	B (wt.%)	C (wt.%)
Carbon	K series	5.59	4.18	-
Titanium	K series	23.99	14.42	0.21
Chromium	K series	-	7.45	4.68
Cobalt	K series	-	6.32	6.25
Nickel	K series	6.31	35.67	64.01
Tantalum	L series	64.11	31.96	5.96
Aluminum	K series	-	-	5.51
Molybdenum	L series	-	-	3.71
Tungsten	L series	-	-	9.67

Table 6. The EDS of points A, B, and C in Fig. 8.

Element	Series	A (wt.%)	B (wt.%)	C (wt.%)
Carbon	K series	10.29	-	-
Titanium	K series	13.47	0.54	2.51
Chromium	K series	-	5.08	6.05
Cobalt	K series	-	8.94	7.90
Nickel	K series	21.02	62.79	56.90
Tantalum	L series	55.22	4.75	9.18
Aluminum	K series	-	7.55	5.37
Molybdenum	L series	-	-	4.06
Tungsten	L series	-	10.36	8.04

The microstructural analysis before and after ECM demonstrates the presence of gamma (γ), gamma prime (γ'), and carbide phases in both cases. The EDS analysis provides quantitative information about the elemental composition of these phases, confirming their identity and distribution in the microstructure.

5. Conclusions

The SEM images and EDS analysis of the CMSX-4 superalloy before and after the ECM process revealed the following:

1. Carbide phases: The large white particles observed in the images are carbide phases that are dispersed heterogeneously throughout the material, both before and after the ECM process.
2. Gamma-prime strengthening phase: The black parts in the images indicate the gamma-prime strengthening phase (γ') within the gamma field phase (γ). These phases are observed as the field gamma phase and the cubic gamma-prime phase.
3. Microstructural integrity: The SEM images show that the sample is free of grain boundaries before and after the ECM machining, indicating that the sample retains its single-crystal structure. Additionally, the gamma-prime cubic phases are also homogeneously distributed at very short distances from each other within the gamma field phase.
4. Microstructural stability: Based on the comparison of the images, the ECM process does not affect the microstructure of the CMSX-4 nickel-based single-crystal superalloy.
5. Lack of defects: The scanning electron microscopy images show that the sample under machining conditions lacks new grain germination or significant defects in the microstructure.

Based on the comparison of the images, the conclusion is that the ECM process does not affect the microstructure of the CMSX-4 nickel-based single-crystal superalloy. The sample remains a single crystal with the gamma-prime phases distributed in the gamma field, and there is no evidence of significant defects in the microstructure.

Declarations

Ethical approval: This manuscript is the authors' own original work, which has not been previously published elsewhere.
Consent to participate: The authors voluntarily agree to participate in this research study.
Consent to publish: The authors consent to the publication of the manuscript in "Journal of Computational and Applied Research in Mechanical Engineering"
Conflicts of interest: The authors declare no competing interests. Also, this manuscript has not been submitted to, nor is it under review at, another journal or other publishing venue.
Funding: The authors received no funding for this work.
Competing interests: The authors declare no competing interests.
Availability of data and materials: The data/materials will be available upon request.

References

[1] T. Bergs and S. Harst, "Development of a process signature for electrochemical machining". *CIRP Ann.*, Vol. 69, No. 1, pp. 153-156, (2020).

[2] A. Mehrvar, M. Motamedi and A. Jamalpour, "Modeling of Jet Electrochemical Machining Using Numerical and Design of Experiments Methods", *Sci. Iran.*, Vol. 31, No. 20, pp. 1880-1888, (2024).

[3] G. Wang, Y. Zhang, H. Li, et al., "Ultrasound-Assisted Through-Mask Electrochemical Machining of Hole Arrays in ODS Superalloy", *Materials*, Vol. 13, No. 24, p. 5780, (2020).

[4] P.B. Tailor, A. Agrawal and S. S. Joshi, "Evolution of electrochemical finishing processes through cross innovations and modelling", *Int. J. Mach. Tool. Manu*, Vol. 66, pp. 15–36, (2013).

[5] A. Mehrvar, A. Basti and A. Jamali, "Optimization of electrochemical machining process parameters: Combining response surface methodology and differential evolution algorithm", *P. I. Mech. Eng. E-J. Pro*, Vol. 231, No. 6, pp.1114-1126, (2016).

[6] A. Mehrvar, A. Basti and A. Jamali, "Modelling and parameter optimization in electrochemical machining process: application of dual response surface-desirability approach", *Lat. Am. Appl. Res*, Vol. 47, No. 4, pp. 157-162, (2017).

[7] S. K. Vaiyapuri, A. Moganraj, et al., "Development of thermal barrier coating on single crystal superalloy CMSX-4 by two-source evaporation EB-PVD and hot corrosion performance of the coating in a simulated aero-engine environment", *Surf. Coat. Technol.*, Vol. 485, p. 130885, (2024).

[8] M. Ramsperger, R.F. Singer and C. Körner, "Microstructure of the nickel-base superalloy CMSX4 fabricated by selective electron beam melting", *Metall. Mater. Trans. A*, Vol. 47, pp. 1469-1480, (2016).

[9] X. Yu, W. Xuan, et al., "An insight into the creep failure mechanism of sliver defect in the second-generation nickel-based single crystal superalloy CMSX-4", *Eng. Fract. Mech.*, Vol. 307, p. 110307, (2024).

[10] T. Cheng, Y. Wang, et al., "Effect of solidification direction on microstructure and mechanical property of single crystal superalloy CMSX-4", *Mater. Charact.*, Vol. 202, p. 112992, (2023).

[11] A. Paraschiv, G. Matache and C. Puscasu, "The effect of heat treatment on the homogenization of CMSX-4 single-crystal Ni-based superalloy", *Transport. Res. Procedia*, Vol. 29 pp. 303-311, (2018).

[12] B. Yin, G. Xie, X. Jiang, et al., "Microstructural Instability of an Experimental Nickel-Based Single-

Crystal Superalloy", *Acta Metall. Sin. Engl. Lett*, Vol. 33, pp. 1433–1441, (2020).

[13] A. Mehrvar and A. Mirak, "Comparative evaluation of surface integrity of CMSX-4 nickel-based superalloy after grinding, wire electrical discharge machining, and electrochemical machining processes", *J. Mater. Eng. Perform.*, Vol. 33, pp. 2616–2622, (2024).

[14] A. Mehrvar, A. Mirak and M. Rezaei, "Numerical and Experimental Investigation of Electrochemical Machining of Nickel-Based Single Crystal Superalloy", *Modares Mechanical Engineering*, Vol. 20, No. 7, pp. 1873-1881, (2020).

[15] A. Mehrvar, M. Motamedi and A. Mirak, "Modeling of electrochemical machining of nickel-based single crystal super alloy by combining numerical and design of experiments methods", *J Solid Fluid Mech*, Vol. 10, No. 3, pp. 207-217, (2020).

[16] F. Klocke, M. Zeis, A. Klink, et al., "Experimental research on the electrochemical machining of modern titanium- and nickel-based alloys for aero engine components", *Procedia CIRP*, Vol. 6, pp. 368-372, (2013).

[17] F. Scherillo, A. Astarita, U. Prisco, et al., "Selective electrochemical machining of the steel molds in hot isostatic pressing of Ti6Al4V powder", *Mater. Manuf. Process*, Vol. 33, No. 14, pp. 1587–1593, (2018).

[18] S. Niu, N. Qu, S. Fu, et al., "Investigation of inner-jet electrochemical milling of nickel-based alloy GH4169/Inconel 718" *Int. J. Adv. Manuf. Technol*, Vol. 93, pp. 2123-2132, (2017).

[19] A. Zhang, Z. Xu, J. Lu, et al., "Improvement of blade platform accuracy in ECM utilizing an auxiliary electrode", *Mater. Manuf. Process*, Vol. 35, No. 9, pp. 951-960, (2020).

[20] Z. Xu, L. Sun, Y. Hu, et al., "Flow field design and experimental investigation of electrochemical machining on blisk cascade passage", *Int. J. Adv. Manuf. Technol*, Vol. 71, pp. 459–469, (2014).

[21] B. Mouliprasanth and P. Hariharan, "Scale effects and a method to evaluate similarity in electrochemical micromachining of Nitinol", *Mater. Manuf. Process*, Vol. 36, No. 1, pp. 39-47, (2020).

[22] Y. Ge, Z. Zhu and D. Wang, "Electrochemical dissolution behavior of the nickel-based cast superalloy K423A in $NaNO_3$ solution", *Electrochim. Acta*, Vol. 253, pp. 379–389, (2017).

[23] F. Wang, J. Yao and M. Kang, "Electrochemical machining of a rhombus hole with synchronization of pulse current and low-frequency oscillations", *J. Manuf. Processes*, Vol. 57, pp. 91–104, (2020).

[24] D.S. Bilgi, V.K. Jain, R. Shekhar, et al., "Electrochemical deep hole drilling in super alloy for turbine application". *J. Mater. Process. Tech*, Vol. 149, No. 1-3, pp. 445–452, (2004).

[25] Y. Wang, Z. Xu, J. Liu, et al., "Study on flow field of electrochemical machining for large size blade", *Int. J. Mech. Sci.*, Vol. 190, p. 106018, (2021).

[26] S.F. Huang and Y. Liu. "Electrochemical micromachining of complex shapes on nickel and nickel-Based superalloys", *Mater. Manuf. Process*, Vol. 29, No. 11-12, pp. 1483-1487, (2014).

[27] M. Burger, L. Koll, E.A. Werner, et al., "Electrochemical machining characteristics and resulting surface quality of the nickel-base single-crystalline material LEK94", *J. Manuf. Processes*, Vol. 14, No. 1, pp. 62–70, (2012).

[28] A. Singh, S. Anandita and S. Gangopadhyay, "Microstructural Analysis and Multi Response Optimization during ECM of Inconel 825 Using Hybrid Approach", *Mater. Manuf. Process*, Vol. 30, No. 7, pp. 842-851, (2015).

[29] Y. Wang, Z. Xu, J. Hu, et al., "Surface integrity analysis of electrochemical machining of γ-TiAl alloys", *Mater.*

Today Commun., Vol. 25, p. 101686, (2020).
[30] Y. Wang, Z. Xu, J. Hu, et al., "Surface integrity analysis of electrochemical machining of γ-TiAl alloys", *Mater. Today Commun.*, Vol. 25, (2020).

How to cite this paper:

A. Mehrvar, AR. Mirak and M. Motamedi, "Microstructural analysis of nickel-based CMSX-4 superalloy after electrochemical machining", *J. Comput. Appl. Res. Mech. Eng.*, Vol. 15, No. 1, pp. 51-61, (2025).

DOI: 10.22061/jcarme.2025.12184.2660

URL: https://jcarme.sru.ac.ir/?_action=showPDF&article=2451